Entropic Colloidal Interactions in Concentrated DNA Solutions

Ritu Verma, J. C. Crocker, T. C. Lubensky, and A. G. Yodh

Department of Physics and Astronomy, University of Pennsylvania, 209 S. 33rd Street, Philadelphia, Pennsylvania 19104
(Received 9 July 1998)

We explore the entropic interactions between a pair of micron-sized colloidal spheres in DNA solutions. By confining the particles in a line-scanned optical tweezer, we directly measured the functional form of the interaction potential with sub-$k_B T$ resolution in samples where the spheres and the polymer coils were of comparable size. The potential is well described by the Asakura-Oosawa depletion model even in the semidilute regime where DNA coils overlap strongly. Its range and depth increase with increasing concentration in a manner consistent with a crossover from a dilute solution of Gaussian coils to the weakly fluctuating semidilute regime dominated by two-point collisions which is unique to semiflexible polymers. [S0031-9007(98)07491-2]

Colloidal suspensions and polymer solutions are two classic soft materials that have been the focus of decades of study, and yet their properties when mixed together are still only poorly understood. These colloid-polymer mixtures exhibit a rich phase behavior which is not only of fundamental interest [1–10] but also of relevance to systems as diverse as motor oils and frozen desserts. The structural and dynamical properties of these complex fluids ultimately depend on the microscopic interactions between the suspension constituents. We present the first direct measurement of the functional form of the depletion interaction between two colloidal spheres in a nonadsorbing polymer background.

Our measurements probe the variations in depth and range of the potential as a function of polymer concentration, spanning the dilute region where individual coils are noninteracting to the semidilute regime where they become entangled. Unlike other force measurements [3,5], our experiments probe a previously unexplored regime where colloid and polymer sizes are comparable. We find that the traditional hard-sphere depletion potential [8,9] for dilute solutions still applies and that it can be extended into the entangled region by rescaling the effective size of the polymer coils. We obtain quantitative measurements of the polymers' osmotic pressure and correlation length above and below the overlap concentration.

A dilute polymer solution can be modeled as an *ideal* gas of hard spheres [8] with a mean size given by the radius of gyration of the individual polymer coils. Unlike hard spheres, polymers in solution can interpenetrate, significantly reducing any effects due to liquid structure. The experimental situation is depicted in Fig. 1(a). The centers of the polymer "spheres" are excluded from a region of thickness R_g surrounding the colloidal particles. When the "depletion zones" surrounding the two spheres overlap, the total volume accessible to the polymer increases, leading to a gain in the system entropy. This produces an attractive interaction between the two spheres.

When the polymer concentration is increased above the critical overlap concentration, C^*, entanglement effects become important. In this semidilute regime the polymer is characterized by a correlation length ξ rather than by R_g. The length scale ξ may be thought of as the average spatial distance between two neighboring entanglement points. Equivalently ξ describes the mean size of a "blob" within which a section of the polymer chain still behaves as an independent coil. If the polymer-colloid interaction is repulsive, a polymer depleted "correlation cavity" with a thickness proportional to ξ [10,11] [see Fig. 1(b)] develops around each sphere, and a depletion attraction still occurs.

We used a model colloid-polymer mixture to probe these interactions as a function of polymer concentration. The polymer in our experiments is bacteriophage lambda DNA (λ-DNA; New England Biolabs Inc.), which is monodisperse and has a 16 μm contour length. The short, cohesive single-stranded ends were first filled in using DNA Polymerase 1 [12] to prevent circularization and dimerization of the chains. The samples were then resuspended in a standard 10 mM TE buffer
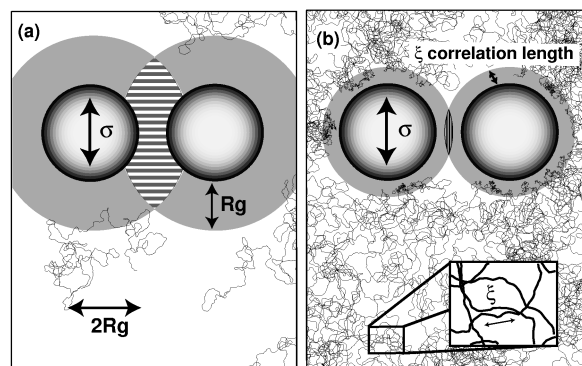

FIG. 1. Polymer depletion in the (a) dilute and (b) semidilute regimes. The depletion region is shaded in grey, and the hatched region corresponds to the increase in volume accessible to the polymers.

(10 mM tris-HCl, 0.1 mM EDTA (ethylenediaminetetra-acetic acid), $pH = 8.0$). In this buffer, λ-DNA has a persistence length of 50 nm [13] and a radius of gyration, measured by light scattering, of $R_g \approx 500$ nm [14]. At this salt concentration, the Debye-Hückel screening length is ≈ 3 nm so that the range of electrostatic inter-actions is much smaller than the entropic length scales we probe.

Our experiments on solutions of λ-DNA were carried out in concentrations ranging from 5 to 300 μg/ml (the overlap concentration is expected to be 30–50 μg/ml [15]). A very small volume fraction ($\approx 10^{-7}$) of nega-tively charged silica spheres of diameter 1.25 $\pm$ 0.05 μm (Bangs Laboratories Inc.) added to the DNA serve as our probe test spheres. The samples are then loaded into a 20 μl microchamber formed by sealing a microscope slide to a No. 1.5 coverslip with a Parafilm spacer, immediately prior to data collection.

We viewed the samples using a Zeiss Axiovert 135 inverted optical microscope with a $100\times$ (NA = 1.4) oil-immersion objective. By focusing about 50 mW of near-infrared light ($\lambda = 1054$ nm) with this objective, we formed an optical tweezer [16]. A galvanometer-driven steering mirror in the light path made it possible to scan the laser focus at 180 Hz along a line in the focal plane. Unable to follow the trap, the colloidal spheres respond to the time-averaged optical field, diffusing freely along the line while being strongly confined in the two perpendicular directions. This confinement to the focal plane is key to our ability to equate the spheres' three-dimensional separation with the measured in-plane separation. Slowing the scan rate near the middle of the line draws each sphere there with a nearly harmonic optical force, speeding data collection while producing an easily subtracted effective pair interaction. Bidirectional scanning also ensures that small "kicks" [16] imparted by the trap nearly cancel out.

Typically we trapped two silica spheres on the line focused 3 μm from the chamber wall. This distance was chosen to minimize both wall effects and out of plane particle motion due to weakening of the trap by spherical aberration. We carefully regulated the sphere-wall separation and laser power during the course of the experiment to keep trapping characteristics constant. The motion of the beads was imaged with a CCD camera (Hitachi, model KP-M1U) and recorded with a computer-controlled S-VHS video deck. After collecting roughly 30 min of tape for a single pair of beads in DNA, the experiment was repeated immediately with a DNA-free buffer sample that served as a control measurement. The resulting 50 000 video frames were then digitized, and corrected for pixel-to-pixel gain variations on the CCD chip. We located the centroids of the silica spheres in each frame with an algorithm that approximately corrects for the overlap of the diffraction blurred images [17].

The probability, $P(r)$, of finding the two spheres with centers separated by r is related to the free en-ergy of the system through the Boltzmann relation,

$P(r) \propto \exp[-U(r)/k_B T]$, where $U(r)$ is the free energy, k_B is the Boltzmann constant, and T is the temperature. We measure the interaction free energy by taking the natural logarithm of the equilibrium probability distri-bution of the two-sphere separations. In addition to the contributions from the entropic interactions we wish to study, the measured free energy contains contributions from the bare interaction of the hard spheres and from small optical tweezer-induced interactions. The DNA-free measurement enables us to independently determine these background forces since the optical properties of the DNA solution, which determine our trap characteristics, do not change noticeably over the range of concentrations used. We isolate the entropic interactions due to the DNA by subtracting off this background potential, which we model with a smooth polynomial fit outside the repulsive core region.

The resulting potentials for all measured DNA concen-trations are displayed in Fig. 2. We adopt the Asakura-Oosawa (AO) depletion model to interpret our data. The AO potential [8] between two spheres of diameter σ, sepa-rated by a distance r, in a dilute solution can be expanded to yield

$$U(r) = -\Pi_p \frac{\pi}{4} \left[\sigma\lambda(r - \sigma\lambda)^2 + \frac{1}{3}(r - \sigma\lambda)^3 \right] \quad (1)$$
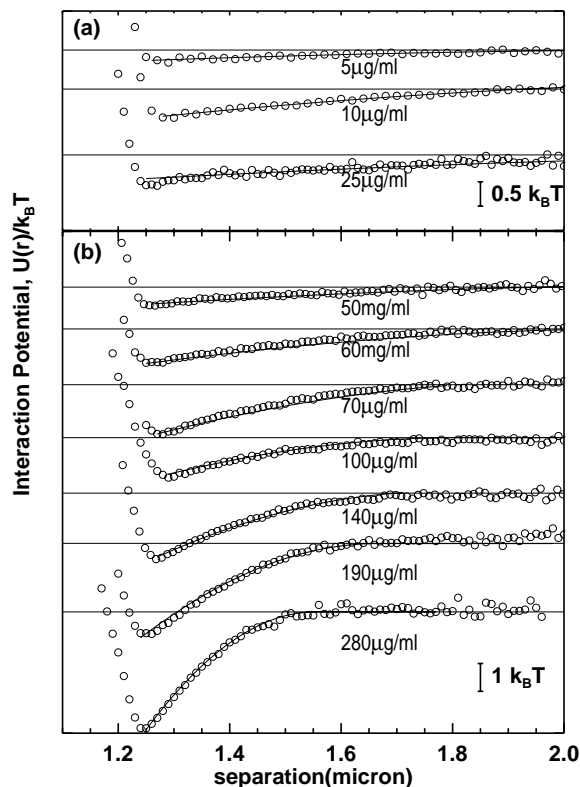

FIG. 2. The interaction potential between two 1.25 μm silica spheres, in (a) the dilute and (b) the semidilute regions. The dimensionless potential $U(r)/k_B T$ is plotted as a function of r, the interparticle distance. The open circles represent actual data points, and the solid lines are fits to the AO model, as described in the text.

for $\sigma \leq r \leq \sigma + 2R_p$ where Π_p is the polymer osmotic pressure, R_p is the effective hard-sphere radius that describes the polymer, and $\lambda = 1 + 2R_p/\sigma$.

As the concentration is increased into the semidilute regime, the potential wells get deeper and the range contracts dramatically. In semidilute solutions the intersphere potential is predicted [10] (within the Derjaguin approximation, i.e., $\sigma \gg \pi\xi$) to be

$$\tilde{U}(r) \approx -\Pi_p \frac{\pi\sigma}{4} [r - (\sigma + \pi\xi)]^2 \qquad (2)$$

for $\sigma \leq r \leq \sigma + \pi\xi$. The potentials $U(r)$ and $\tilde{U}(r)$ are identical to lowest order in $[r - (\sigma + 2R_p)]$ in the limit $\sigma \gg 2R_p$ provided R_p is identified with $(\pi/2)\xi$. In the semidilute regime, the third-order term is small, and the AO model is nearly identical to $\tilde{U}(r)$. The AO model therefore provides a good description of the potential in the dilute as well as the semidilute regime. The success of the AO model in the semidilute solution can be understood as due to the background fluid resembling a system of uncorrelated blobs of size proportional to ξ.

We fit our measured potentials with Eq. (1) (shown in Fig. 2 as solid lines), treating Π_p and R_p, as free parameters. Since our method only determines the potential up to an undetermined additive offset, we shift the curves vertically so that the potential at long range is zero.

To understand the concentration dependence of Π_p and R_p we briefly review some polymer theory [11,18]. A polymer of length L and persistence length l_p can be viewed as a chain with $N_{\rm eff} \equiv L/2l_p$ links. Semiflexible polymers have persistence lengths that are larger than the link diameter d, and they are characterized by a rigidity parameter $p \equiv 2l_p/d \gg 1$ (for DNA, $p \approx 50$). In a θ solvent, a polymer chain is described by a random walk with Gaussian statistics and has an end-to-end separation $R_{\rm ideal} = 2N_{\rm eff}^{1/2}l_p$. The strength of self-avoiding interactions away from this point can be characterized by the second virial coefficient $B \sim dl_p^2\tau$, where τ is the solvent quality. As τ increases from zero, there is a crossover from ideal behavior with $R \sim N_{\rm eff}^{1/2}$ to swollen behavior with $R \sim N_{\rm eff}^{3/5}$ at $z \equiv 2(3/2\pi)^{3/2}N_{\rm eff}^{1/2}B/l_p^3 \sim 1$. The virial expansion for the pressure Π_p at small polymer coil concentration, n_p, is given by $\Pi_p/k_BT = n_p + BN_{\rm eff}^2 n_p^2$.

As link concentration $c = pN_{\rm eff}n_p$ is increased, three distinct semidilute regimes emerge in semiflexible polymers. These regimes are distinguished by the dependence of the correlation length and osmotic pressure on concentration. The three regimes, labeled, respectively, IV, VI, and V in Refs. [11,19], are the strongly fluctuating regime (IV) in which $\Pi_p \sim \tau^{3/4}p^{3/4}c(cd^3)^{5/4}$ and $\xi \sim d(cd^3)^{-3/4}\tau^{-1/4}p^{-1/4}$, a weakly fluctuating regime dominated by pairwise contacts (VI) with $\Pi_p \sim d^3\tau c^2$ and $\xi \sim dp^{1/2}\tau^{-1/2}(cd^3)^{-1/2}$, and a weakly fluctuating regime (V) dominated by triple contacts with $\Pi_p \sim d^6c^3$ and $\xi \sim dp^{1/2}(cd^3)^{-1}$. Region IV is normally referred to as the semidilute regime in flexible polymers.

In region (VI) the polymer osmotic pressure and the correlation length can be described by mean-field theory [11,19] and are given by $\Pi_p/k_BT = BN_{\rm eff}^2 n_p^2$ and $\xi = l_p(6BN_{\rm eff}n_p)^{-1/2}$. For semiflexible polymers with $z > 1$, a concentration increase results in a transition from dilute swollen chains to the strongly fluctuating semidilute region (IV) and then to the weakly fluctuating region (VI). However, when $z < 1$ (but not too small), there is a direct crossover from Gaussian chains to the weakly fluctuating region (VI) with increasing concentration. As we shall see, our data yield $z \approx 0.25$ and provide strong evidence for the latter crossover.

In the dilute solution the effective polymer radius R_p should equal the radius of gyration of the polymer, R_g, and the fitted osmotic pressure should depend linearly on DNA concentration, n_p (i.e., $\Pi_p = n_p k_B T$). The first three data points in Figs. 3(a) and 3(b) correspond to the
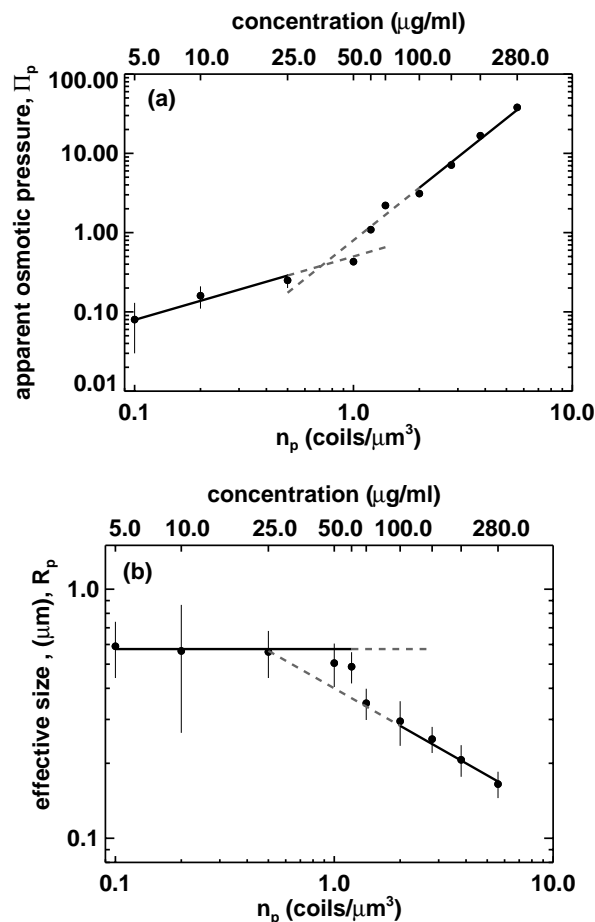

FIG. 3. In (a) we present the scaling behavior of the osmotic pressure vs the concentration. The vertical axis represents $\Pi/k_B T$, and the horizontal axis is concentration in units of number density. Similarly in (b) the filled circles represent the fit parameter R_p [we have used $\xi = (2/\pi)R_p$ in the semidilute regime] in microns, plotted against different polymer concentrations. The solid lines represent fits to mean-field theory predictions and are described in detail in the text. In both graphs $n_p^* \approx (4\pi/3)R_p^{-3} \approx 1.0$ $\mu{\rm m}^{-3}$ marks the crossover from the dilute to the semidilute regime.

parameters of the dilute regime. The measured effective diameter of 1.1 ± 0.2 μm is independent of concentration and agrees well with light scattering measurements for R_g [14] in similar buffers. The osmotic pressure displays a nearly linear behavior, although the measured prefactor of 0.5 ± 0.3 obtained for this fit deviates from the expected hard-sphere value of unity. The relatively large error for the parameters in the dilute limit is a result of the shallow well depth of the interaction curves, whose long range also tends to increase the uncertainty in determining their vertical offset. Alternatively this discrepancy could be due to the nonspherical nature of the polymer coils or polymer-polymer interactions as suggested in Refs. [4] and [7].

The behavior of the interaction potentials changes dramatically in the semidilute regime. Beyond the critical concentration, a best fit to the data yields $R_p = (0.4 \pm 0.05)n_p^{-0.5 \pm 0.1}$, and $\Pi_p/k_{\mathrm{B}}T = (0.8 \pm 0.2)n_p^{2.2 \pm 0.2}$ where R_p is measured in μm and n_p and $\Pi_p/k_{\mathrm{B}}T$ in $(\mu\text{m})^{-3}$. The relationship between the "effective size" and n_p has a measured scaling exponent of -0.5 ± 0.1 suggesting that our solution lies in the weakly fluctuating semidilute regime (VI), and excludes the $-3/4$ exponent predicted for the strongly fluctuating semidilute region (V). In contrast, the measured exponent of 2.2 ± 0.2 for Π_p as a function of n_p does not allow us to differentiate the predictions of 2.25 for the strongly fluctuating regime from the value of 2 for the weakly fluctuating region. Our data combined with the calculated value of $z = 0.25 < 1$ in dilute solutions is most consistent with a crossover as a function of concentration from the dilute Gaussian chain region to the weakly fluctuating semidilute region (VI) for semiflexible polymers.

The second virial coefficient for λ-DNA is measured from the slope of the osmotic pressure data to be $B = 3.1 \pm 0.8 \times 10^{-5}$ μm^3 [20]. This result also provides a useful consistency test of the interpretation of our data. We can compare the measured correlation length $\xi_m = (2/\pi)R_p$ with the theoretically predicted correlation length $\xi_t = l_p(6BN_{\mathrm{eff}}n_p)^{-1/2}$ that can be calculated using the measured B. This predicts that $\xi_t n_p^{1/2} = (0.28 \pm 0.03)$ μm$^{1/2}$ is consistent with $\xi_m n_p^{1/2} = (0.25 \pm 0.03)$ μm$^{1/2}$. This also strongly suggests that our substitution of $(\pi/2)\xi$ for R_p in Eq. (1) is appropriate.

We have presented the first simultaneous measurements of the range and depth of the interaction potential between two colloidal particles in a polymer solution of varying concentrations, including a regime where the semiflexible chains are strongly entangled. In that case, our results can be successfully modeled by an AO theory where the polymer behaves as a gas of uncorrelated hard spheres of size ξ. Our *model independent* potentials serve as an exemplar for the microscopic investigation of a broad range of questions that commonly arise in nanometer scale solutions where both polymers and colloids are often of comparable size. We also observe strong evidence for transitions to the weakly fluctuating regime dominated by

pairwise contacts that is unique to semiflexible polymers. The technique we have demonstrated provides an effective way of probing colloidal interactions in complex fluids and opens up possibilities for future investigation of the polymer fluctuation spectrum.

---

[1] H. M. Schaink and J. A. M. Smit, J. Chem. Phys. **107**, 1004 (1997); E. Eisenriegler, A. Hanke, and S. Dietrich, Phys. Rev. E **54**, 1134 (1996); E. J. Meijer and D. Frenkel, J. Chem. Phys. **100**, 6873 (1994); T. Odjik, J. Chem. Phys. **106**, 3402 (1997); P. Richmond and M. Lal, Chem. Phys. Lett. **24**, 594 (1974).

[2] E. Evans and D. Needham, Macromolecules **21**, 1822 (1988); H. N. W. Lekkerkerker, W. C.-K. Poon, P. N. Pusey, A. Stroobants, and P. B. Warren, Europhys. Lett. **20**, 559 (1992); D. Rudhart, C. Bechinger, and P. Leiderer, Phys. Rev. Lett. **81**, 1330 (1998).

[3] A. J. Milling and S. Biggs, J. Colloid Interface Sci. **170**, 604 (1995).

[4] X. Ye, T. Narayanan, P. Tong, and J. S. Huang, Phys. Rev. Lett. **76**, 4640 (1996); X. Ye *et al.,* Phys. Rev. E **54**, 6500 (1996).

[5] Y. N. Ohshima *et al.,* Phys. Rev. Lett. **78**, 3963 (1997).

[6] P. Kekicheff, F. Nallet, and P. Richetti, J. Phys. II (France) **4**, 735 (1994).

[7] A. P. Chatterjee and K. S. Schweizer (to be published).

[8] S. Asakura and F. Oosawa, J. Polym. Sci. **33**, 183 (1958).

[9] A. Vrij, Pure Appl. Chem. **48**, 471 (1976).

[10] J. F. Joanny, L. Leibler, and P. G. DeGennes, J. Polym. Sci. **17**, 1073 (1979).

[11] A. Y. Grosberg and A. R. Khokhlov, *Statistical Physics of Macromolecules* (AIP Press, New York, 1994).

[12] J. Sambrook, E. F. Fritsch, and T. Maniatis, *Molecular Cloning—A Lab Manual* (Cold Spring Harbor Lab Press, New York, 1989), 2nd ed.

[13] W. H. Taylor and P. J. Hagerman, J. Mol. Biol. **212**, 363 (1990).

[14] R. L. Schmidt, Biopolymers **12**, 1427 (1973); J. R. Dawson and J. A. Harpst, Biopolymers **10**, 2499 (1971); A. V. Arutyunyan, M. A. Ivanova, D. I. Kurlyand and V. A. Noskin, Mol. Biol. **27**, 705 (1993).

[15] N. Pernodet and B. Tinland, Biopolymers **42**, 471 (1997).

[16] D. Grier, Curr. Opin. Colloid Interface Sci. **2**, 264 (1997); L. P. Faucheux, G. Stolovitzky, and A. Libchaber, Phys. Rev. E **51**, 5239 (1995).

[17] J. C. Crocker, A. D. Dinsmore, J. Matteo, and A. G. Yodh (to be published).

[18] P.-G. DeGennes, *Scaling Concepts in Polymer Theory* (Cornell University Press, Ithaca, 1979).

[19] D. W. Schaefer, J. F. Joanny, and P. Pincus, Macromolecules **13**, 1280 (1980).

[20] Our second virial coefficient can be converted to more conventional units defined by $A_2 = N_A B N_{\mathrm{eff}}^2/M_w^2$. This yields $A_2^{\Pi} = 4.8 \pm 1.2 \times 10^{-4}$ mol cm^3/g^2.